Electronic Supplementary Information

# New fluorescent pH optrodes based on covalently linkable PET rhodamines.

Daniel Aigner[a], Sergey M. Borisov[a,*], Francisco J. Orriach Fernández[b], Jorge F. Fernández Sánchez[b], Robert Saf[c] and Ingo Klimant[a]

[a]Institute of Analytical Chemistry and Food Chemistry, Graz University of Technology, Stremayrgasse 9, A-8010 Graz, Austria

[b]Environmental, Biochemical and Foodstuffs Analytical Control Research Group, Universidad de Granada, Campus de Fuentenueva, E-18071 Granada, Spain

[c]Institute for Chemistry and Technology of Materials, Graz University of Technology, Stremayrgasse 9, A-8010 Graz, Austria

[*]Corresponding author. Tel.: +4331687332516; Fax.: +4331687332502; E-Mail.: sergey.borisov@tugraz.at

UV/Vis spectra

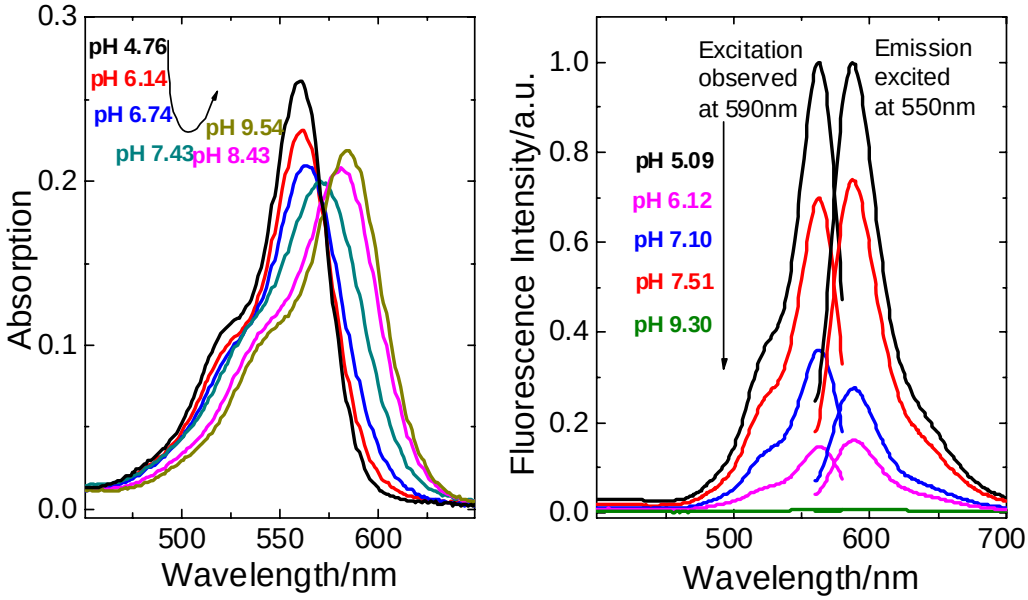


Figure S1: Absorption spectra (left) and fluorescence spectra (right) of **2** in aqueous buffer solution (ionic strength 100mM) at different pH. Dye concentration was 2µM when recording absorption and 0.05µM when recording fluorescence spectra.

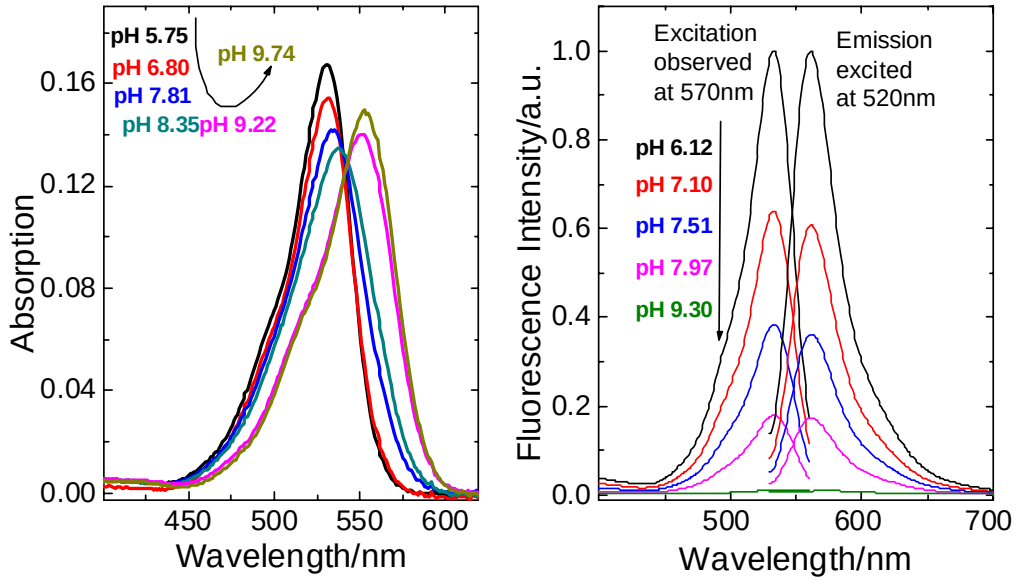


Figure S2: Absorption spectra (left) and fluorescence spectra (right) of **3** in aqueous buffer solution (ionic strength 100mM) at different pH. Dye concentration was 2µM when recording absorption and 0.05µM when recording fluorescence spectra.

Sensor response curves

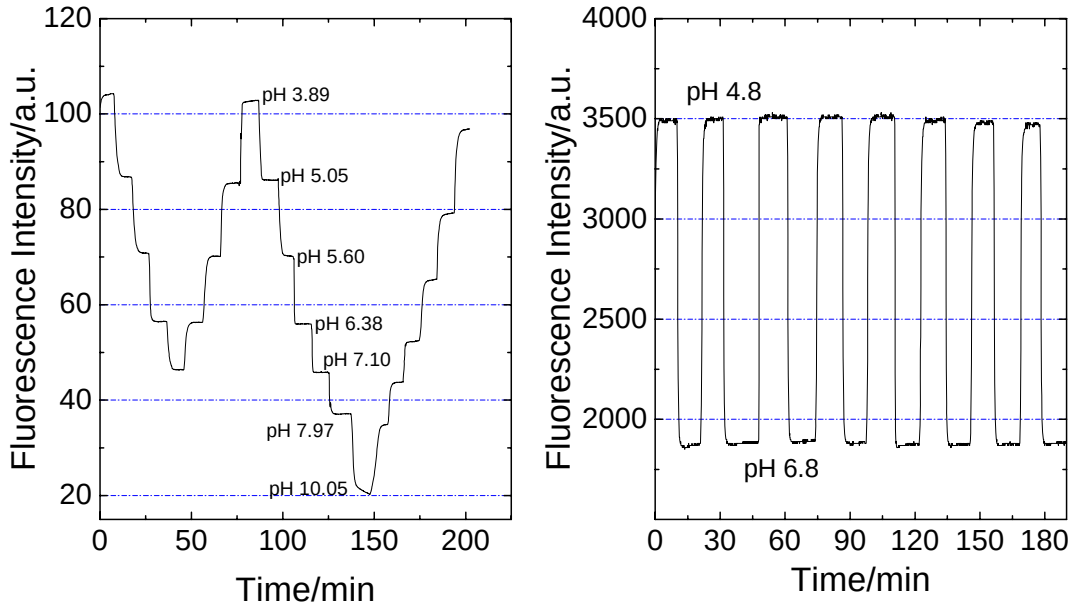


Figure S3: Reversibility and repeatability of the sensor based on silica gel beads in D4® hydrogel. Signal drift and irreversible response are only observed at high pH values (>8) which are essentially outside the sensitive range.

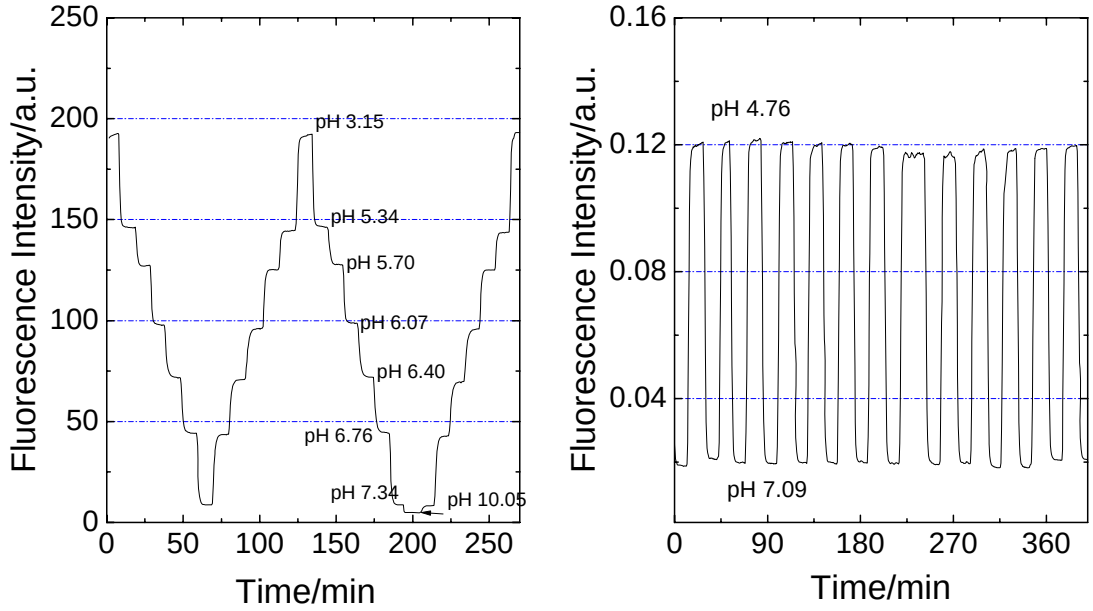


Figure S4: Reversibility and repeatability of the sensor based on cross-linked poly(HEMA) beads linear poly(HEMA). They are good over the whole investigated pH range (pH 3-10).

Calibration

The following sigmoidal function was used for sensor calibration:

$$I = \frac{A_{\min} - A_{\max}}{1 + e^{(pH - pK_a)/dx}} + A_{\max}, \qquad \text{(Equation 1)}$$

where I - fluorescence intensity, $A_{max}$, $A_{min}$, $pK_a$ and $dx$ are numerical coefficients.

NMR spectra

Compound **1**

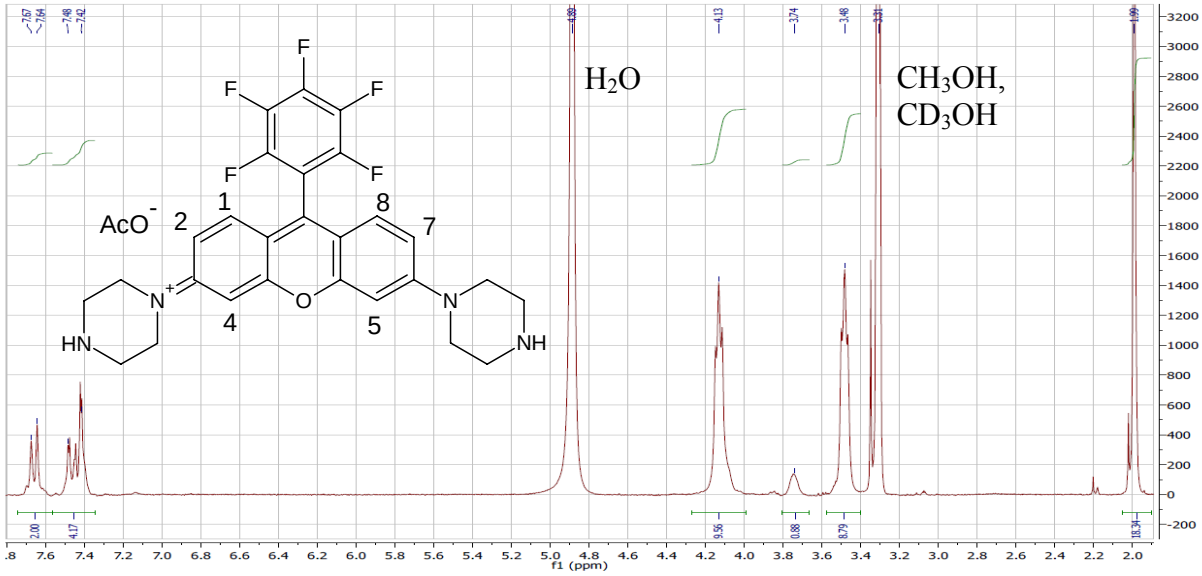


Figure S5: $^{1}$H-NMR spectrum of **1** in $CD_3OD$ containing 0.1% HOAc and 0.1% $CF_3COOH$. Before addition of HOAc the integral of acetate hydrogen (1.99ppm) was 2.9 (spectrum not shown here). δ = 7.65ppm (2H, d, Ar-H(positions 1,8), $J_{ArH12,78}$ = 9.6 Hz); δ = 7.46 (2H, dd, Ar-H(2,7), $J_{ArH24,57}$ = 2.5 Hz); δ = 7.42 (2H, d, Ar-H(4,5)); δ = 4.13 (8H, t, $ArNCH_2$, J = 5.2 Hz); δ = 3.48 (8H, t, $HNCH_2$); δ = 1.99 (3H, s, $H_{acetate}$).

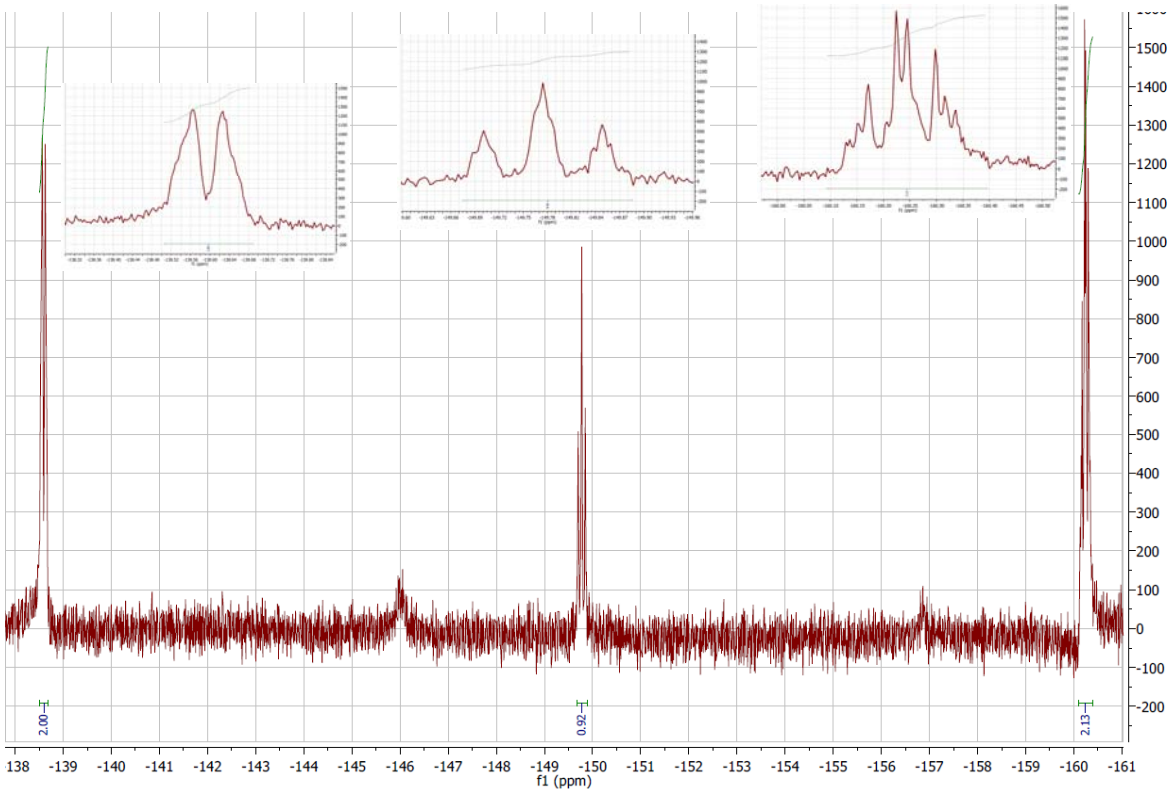


**Figure S6: $^{19}$F-NMR spectrum of 1. δ = -139ppm (2F, d, J = 20 Hz); δ = -150 (1F, t, J = 21 Hz); δ = -160 (2F, dt, $J_1$ = 6 Hz, $J_2$ = 21 Hz).**

Compound **2**

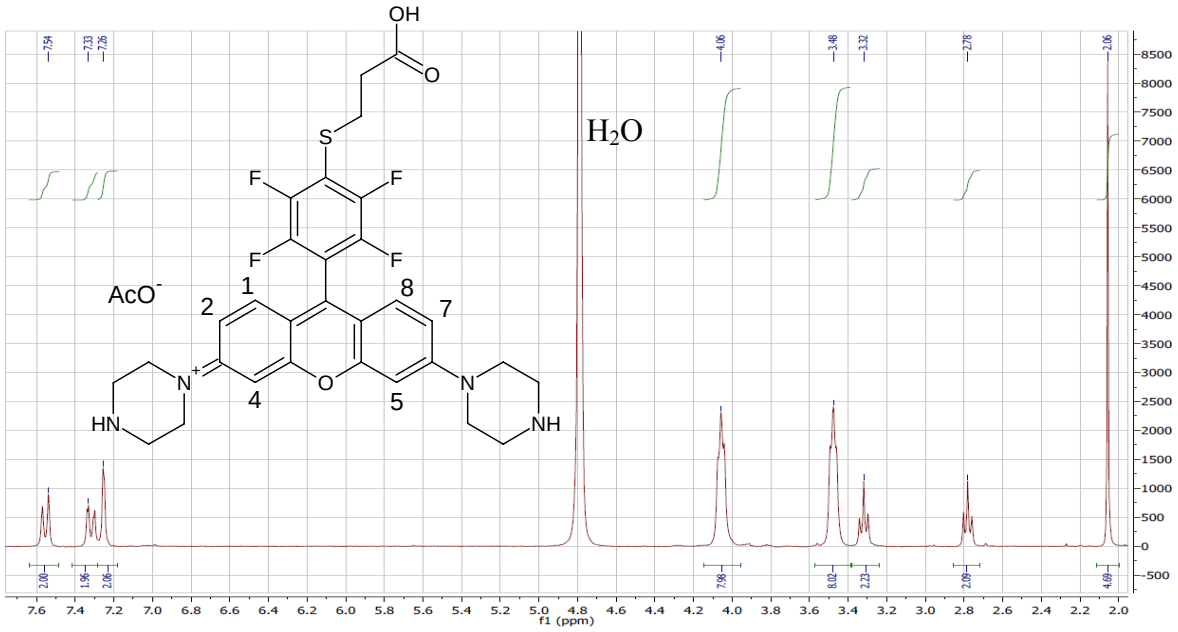


Figure S7: $^{1}$H-NMR spectrum of **2** in $D_2O$ containing 0.1% $CF_3COOH$. δ = 7.55ppm (2H, d, Ar-H(positions 1,8), $J_{ArH12,78}$ = 9.6 Hz); δ = 7.32 (2H, dd, Ar-H(2,7), $J_{ArH24,57}$ = 2.3 Hz); δ = 7.26 (2H, d, Ar-H(4,5)); δ = 4.06 (8H, t, $ArNCH_2$, J = 4.9 Hz); δ = 3.48 (8H, t, $HNC\underline{H_2}$); δ = 3.32 (2H, t, $ArSCH_2$, J = 6.7 Hz); δ = 2.76 (2H, t, $C\underline{H_2}COOH$); δ = 2.06 (4.7H, s, $H_{acetate}$).

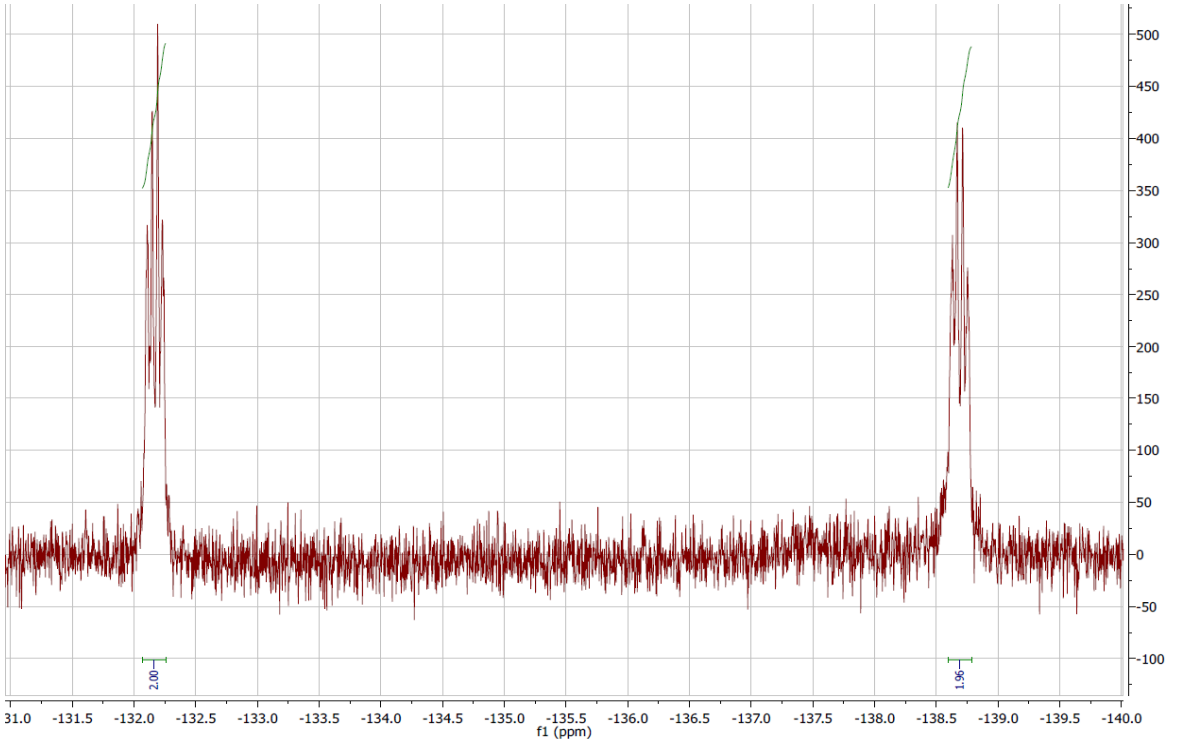


**<u>Figure S8: $^{19}$F-NMR spectrum of 2. δ = -132ppm (2F, q, J = 11 Hz); δ = -139 (2F, q, J = 11 Hz).</u>**

Compound **3**

Compound **3** could be identified as the pure 4'-carboxy regioisomer (figure S9). For comparison, the spectrum of the 5'-carboxy regioisomer (figure S10), which was also obtained upon HPLC purification of crude **3**, is shown. Resonance at >7.9ppm is can be attributed to the protons in the dicarboxyphenyl ring which are in ortho-position to a carboxy group. The 4'-isomer contains only two such protons, while three can be found for the 5'-isomer.

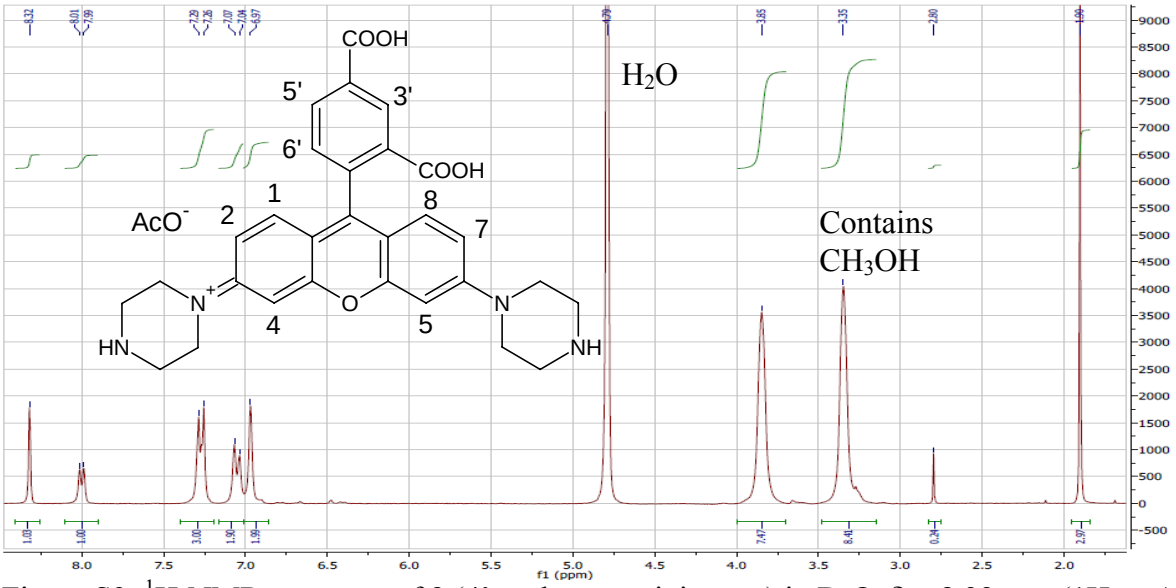


Figure S9: $^{1}$H-NMR spectrum of **3** (4'-carboxy regioisomer) in $D_2O$. δ = 8.32ppm (1H, s, Ar-H(position 3')); δ = 8.00 (1H, d, Ar-H(5'), $J_{ArH5'6'}$ = 7.5 Hz); δ = 7.27 (3H, d, Ar-H(6',1,8), $J_{ArH12,78}$ = 9.3 Hz); δ = 7.06 (2H, d, Ar-H(2,7)); δ = 6.97 (2H, s, Ar-H(4,5)); δ = 3.85 (8H, broad s, $ArNCH_2$); δ = 3.35 (8H, broad s, $HNC\underline{H}_2$); δ = 1.90 (3H, s, $H_{acetate}$).

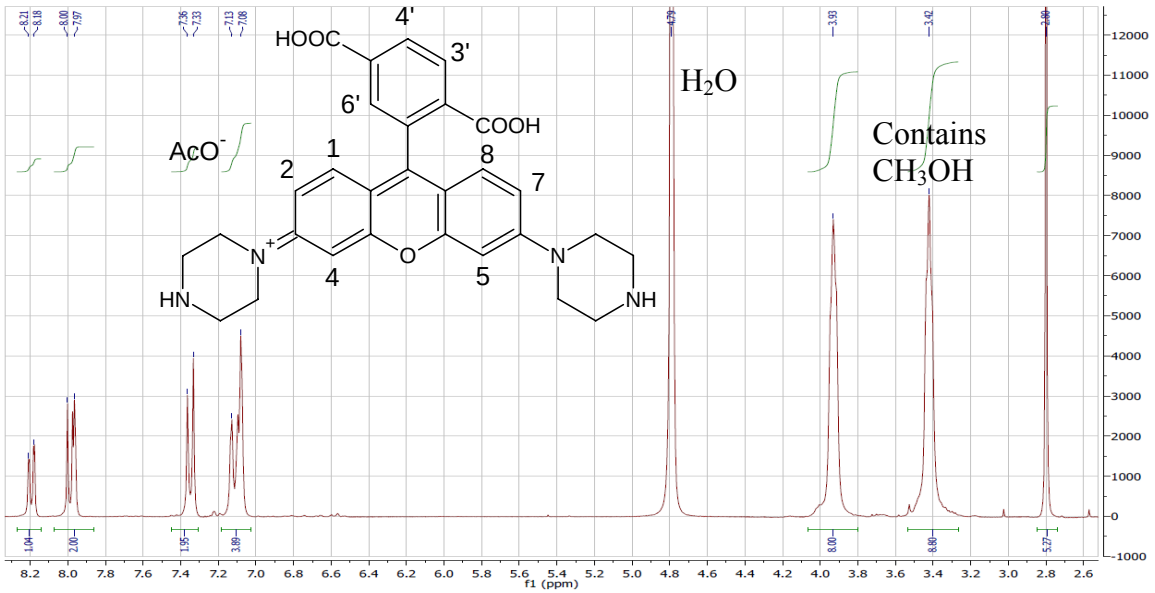


Figure S10: $^{1}$H-NMR spectrum of the 5'-carboxy regioisomer to **3** in $D_2O$. δ = 8.20 (1H, dd, Ar-H(4'), $J_{ArH3'4'}$ = 8.1Hz, $J_{ArH4'6'}$ = 1.7 Hz); δ = 7.99 (1H, d, Ar-H(3')); δ = 7.97 (1H, d, Ar-H(6')); δ = 7.35 (2H, dd, Ar-H(1,8), $J_{ArH12,78}$ = 9.4 Hz, $J_{ArH24,57}$ = 1.6 Hz); δ = 7.11 (2H, d, Ar-H(2,7)); δ = 7.08 (2H, d, Ar-H(4,5)); δ = 3.93 (8H, t, $ArNCH_2$, J = 4.6 Hz); δ = 3.42 (8H, t, $HNC\underline{H}_2$); δ = 2.80 (5.3H, s, $H_{acetate}$).

LC-MS measurements:

Compound **1** after HPLC purification

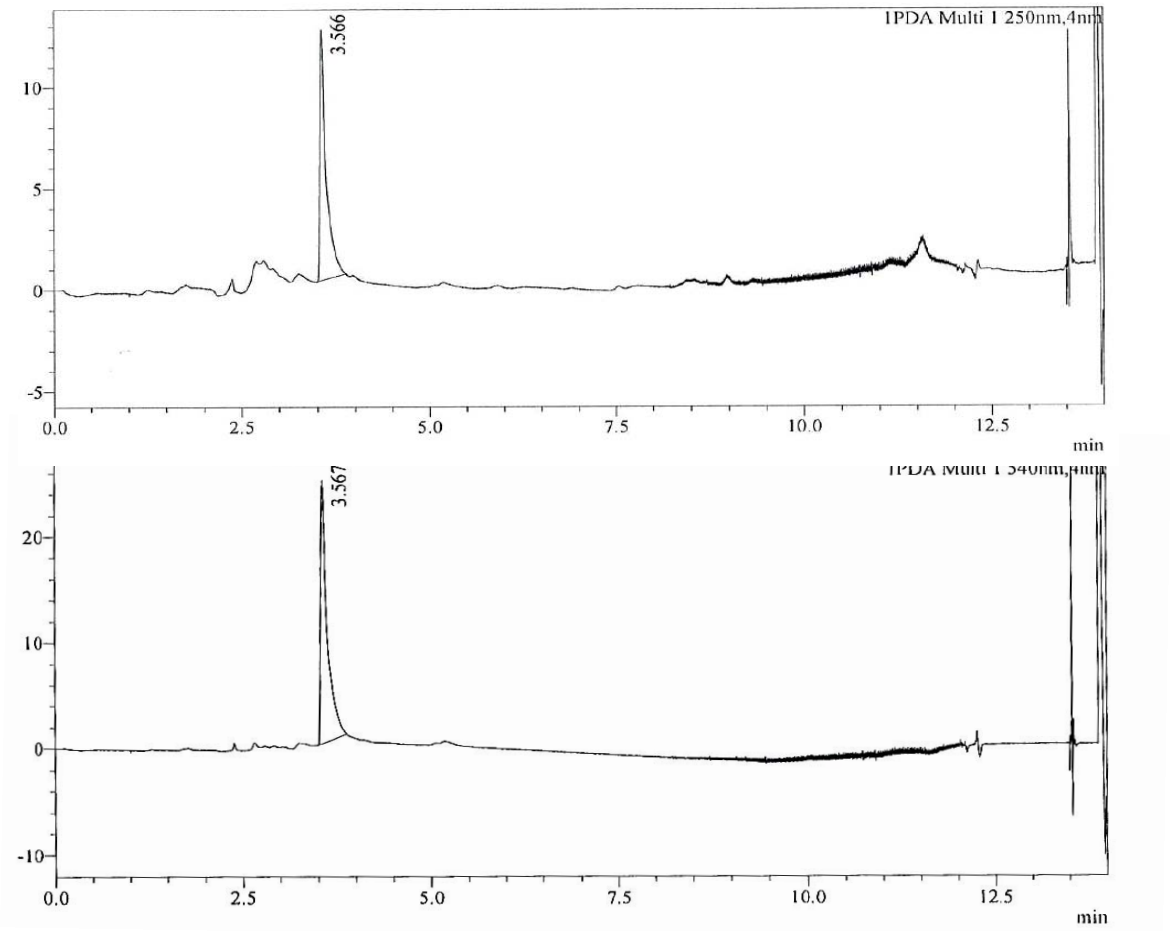


Figure S11: Chromatogram of **1** after HPLC purification, recorded with an UV/VIS detector set to 250nm (top) and 540nm (bottom), bandwidth 4nm each.

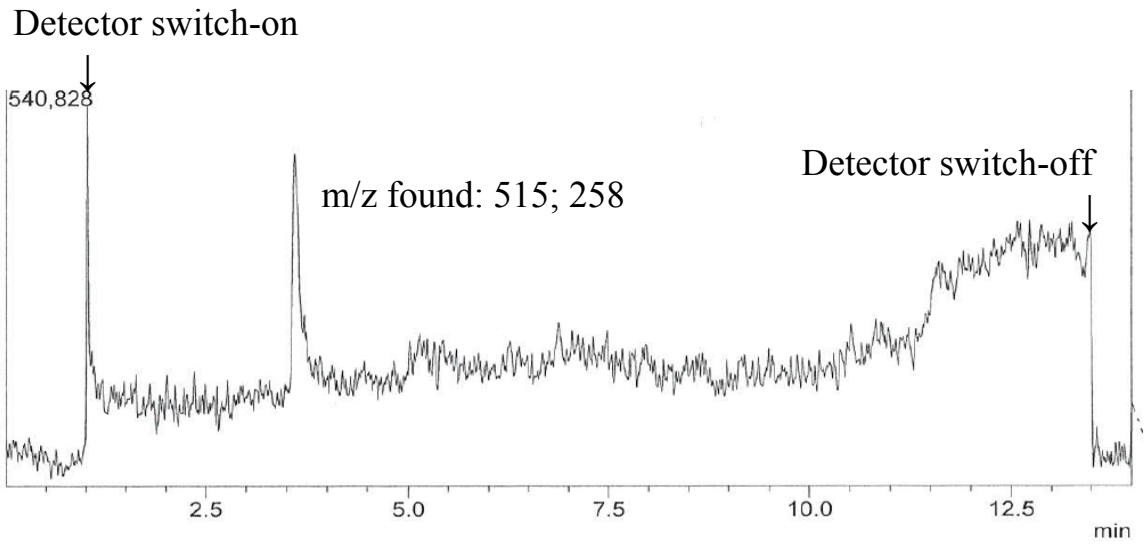


Figure S12: Total ion current chromatogram of **1** after HPLC purification, recorded with an ESI-quadruple MS detector.

Compound **1** (crude)

LC-MS characterisation of crude **1** reveals an interesting side-product which shows a slightly higher mass than the main product but no absorption typical for rhodamines. This could be the product of a reduction (formal addition of $H^-$ to the chinoid form of the rhodamine) which results in disruption of the xanthene chromophore.

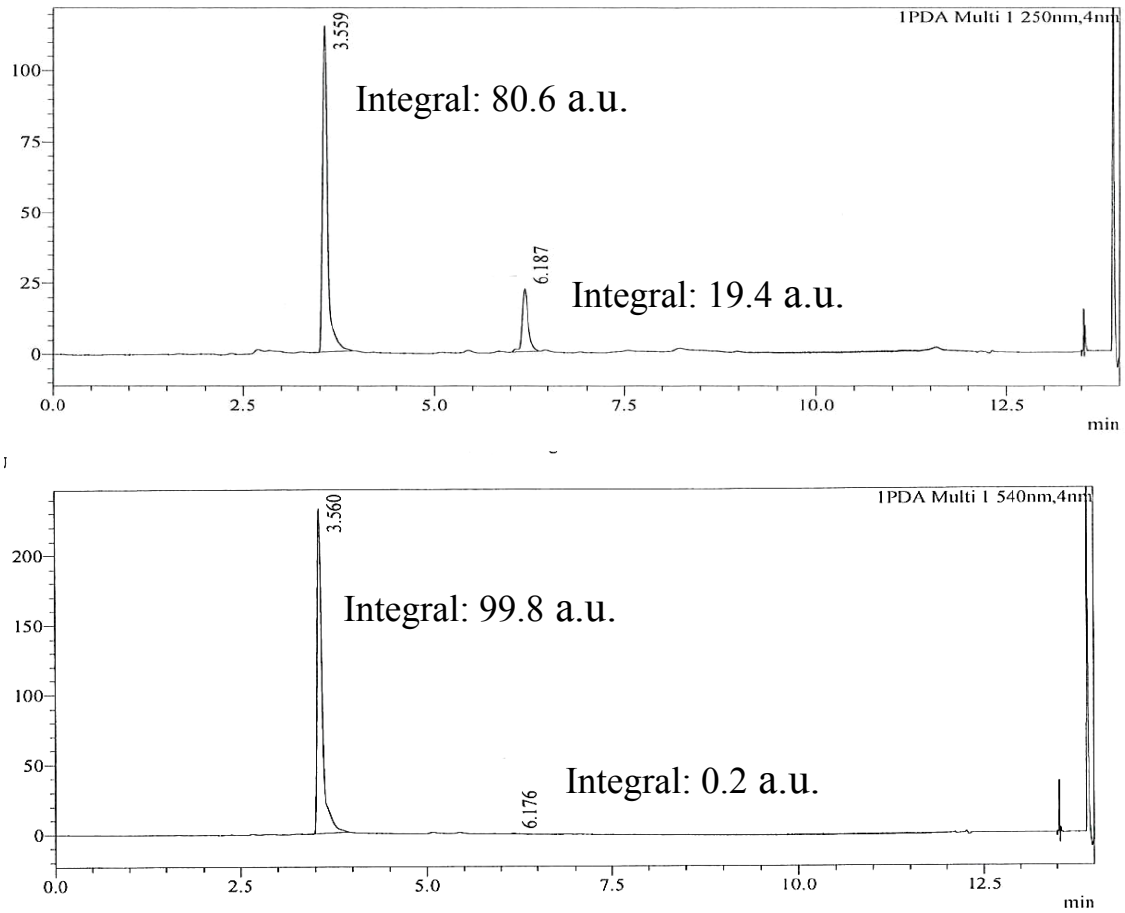


Figure S13: Chromatogram of crude **1**, recorded with an UV/VIS detector set to 250nm (top) and 540nm (bottom), bandwidth 4nm each.

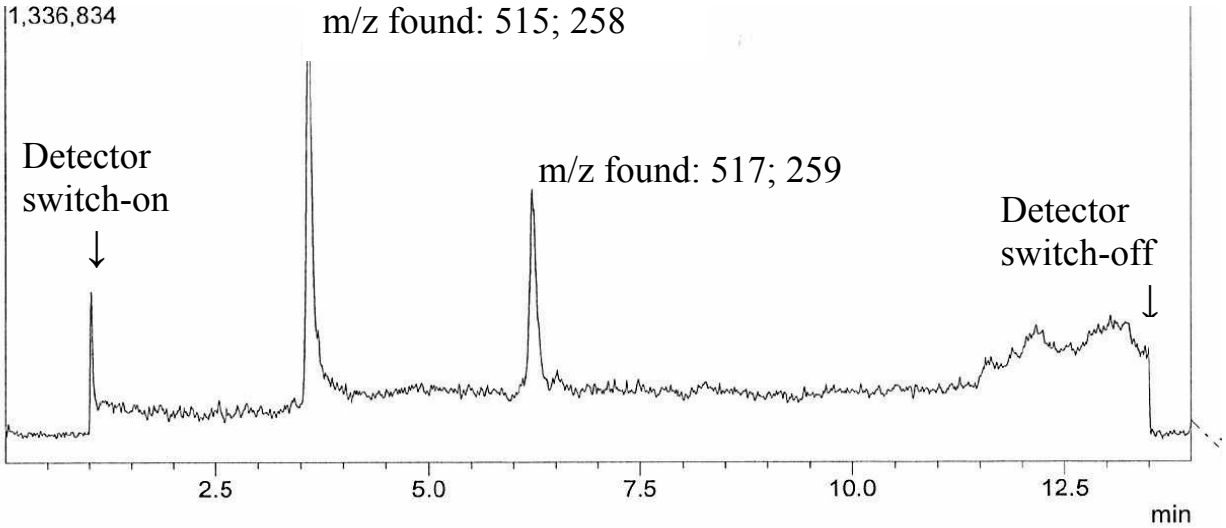


Figure S14: Total ion current chromatogram of crude **1**, recorded with an ESI-quadruple MS detector.

Compound **2** after HPLC purification

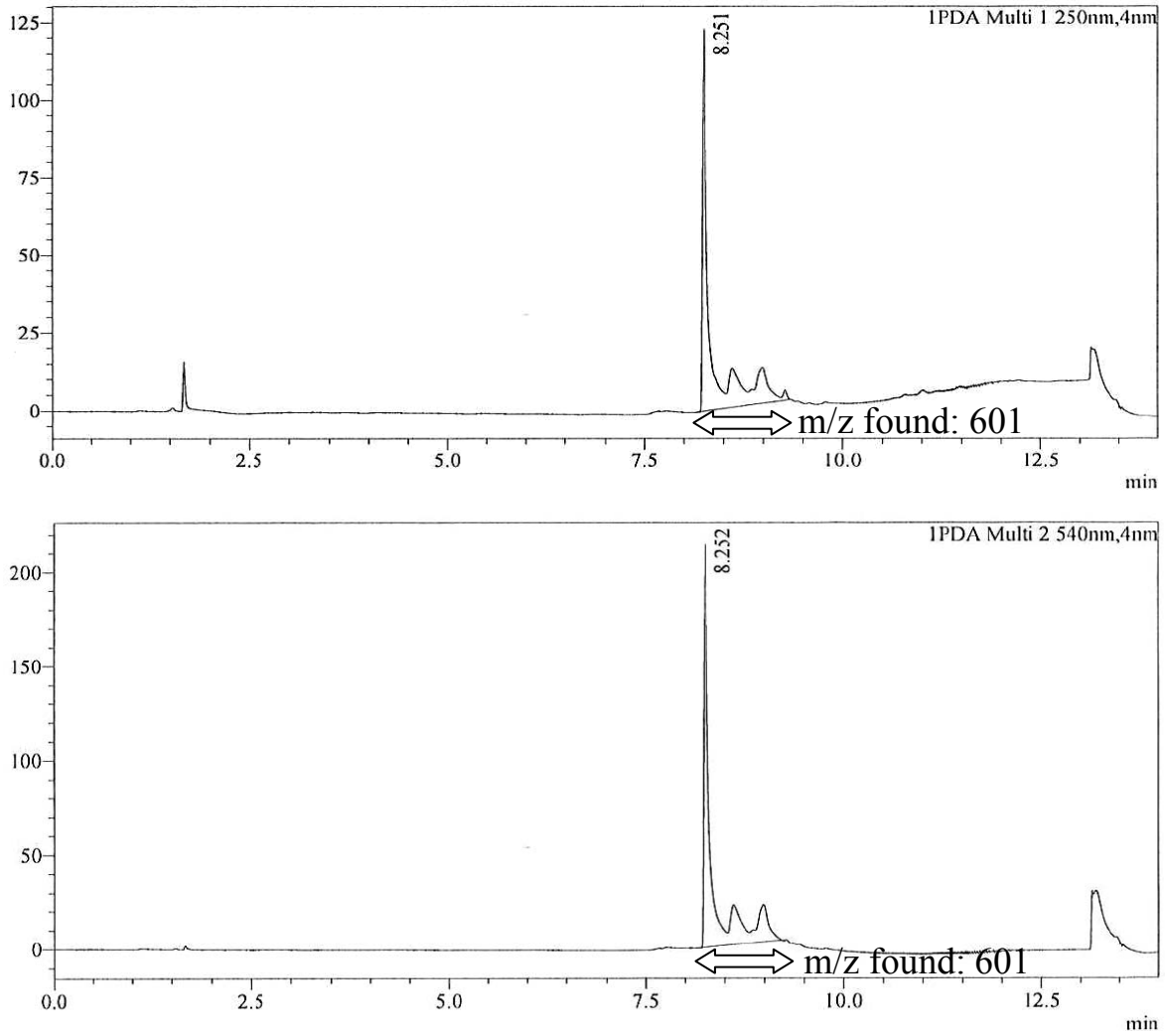


Figure S15: Chromatogram of **2** after HPLC purification, recorded with an UV/VIS detector set to 250nm (top) and 540nm (bottom), bandwidth 4nm each. m/z=601 was found over the whole indicated time (ESI-quadruple MS detector).

Compound **3** after HPLC purification

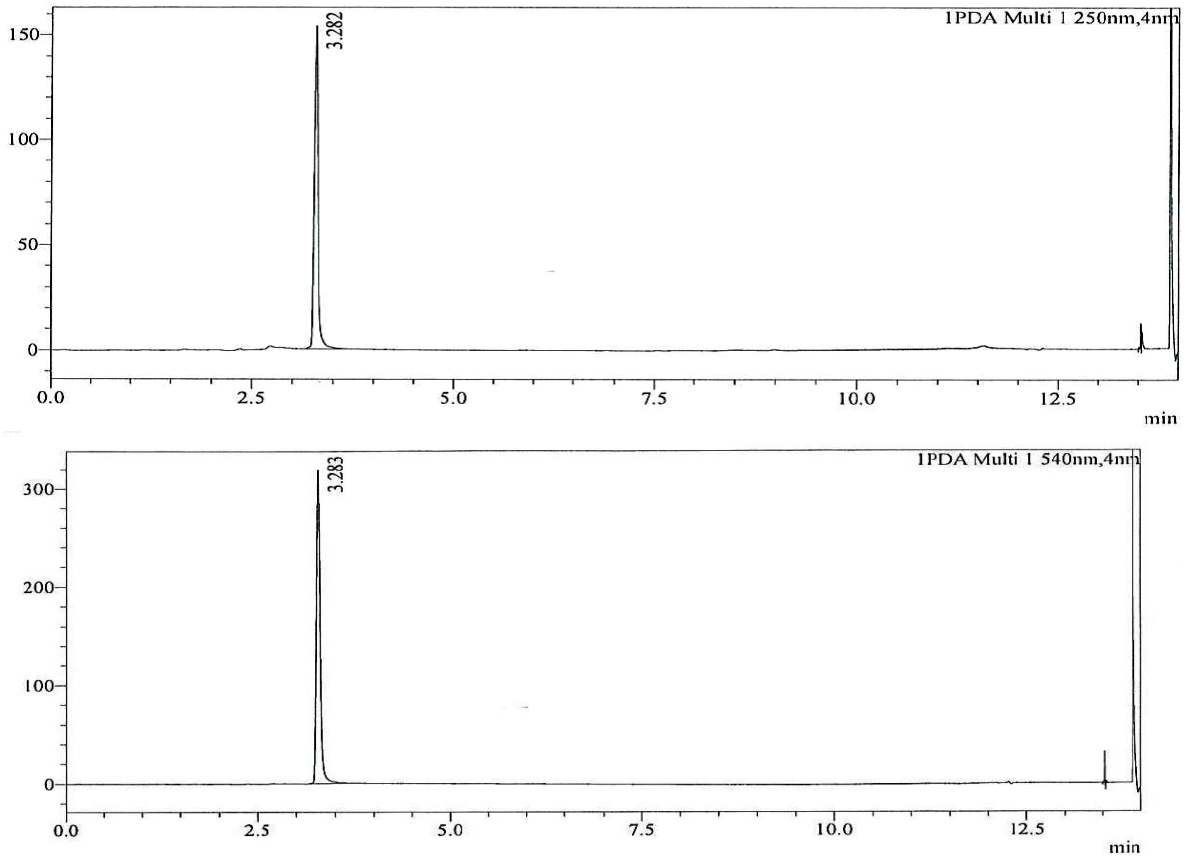


Figure S16: Chromatogram of **3** after HPLC purification, recorded with an UV/VIS detector set to 250nm (top) and 540nm (bottom), bandwidth 4nm each.

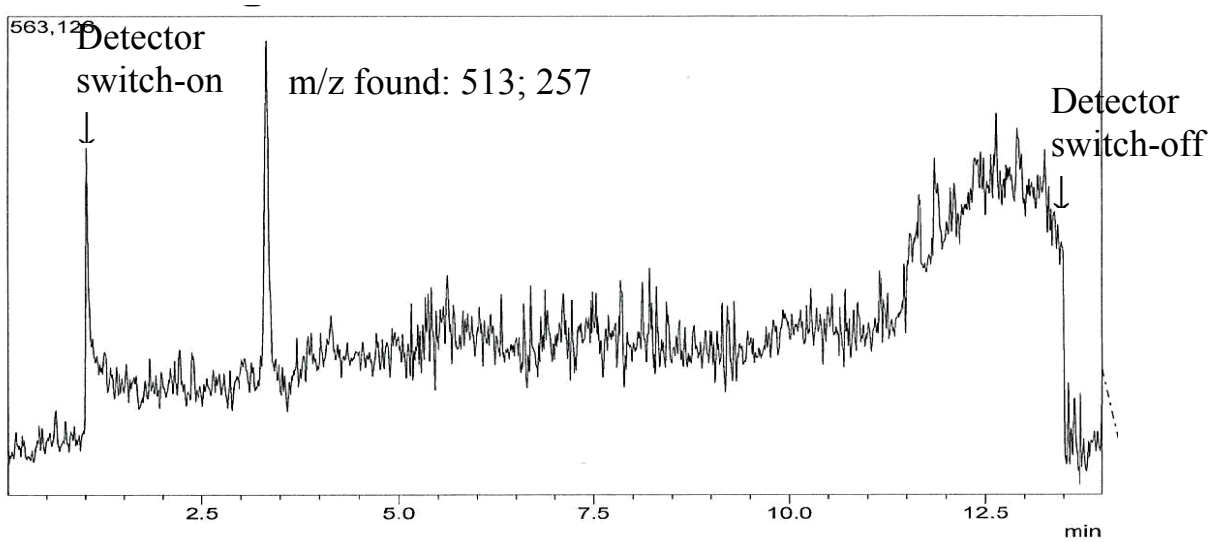


Figure S17: Total ion current chromatogram of **3** after HPLC purification, recorded with an ESI-quadruple MS detector.

Compound **3** (crude)

LC-MS characterisation shows that crude **3** is composed of four different rhodamines which have been formed in an approximate ratio of 1:1:0.3:0.3. The two main components which are eluted earlier have been isolated and identified by NMR spectroscopy as the 5'-carboxy and the 4'-carboxy regioisomers of the target structure. The 4'-isomer (i.e. compound **3**) was used for characterisation. The two components eluted later have higher molecular masses and could be the result of methylation by methanesulfonic acid upon preparation.

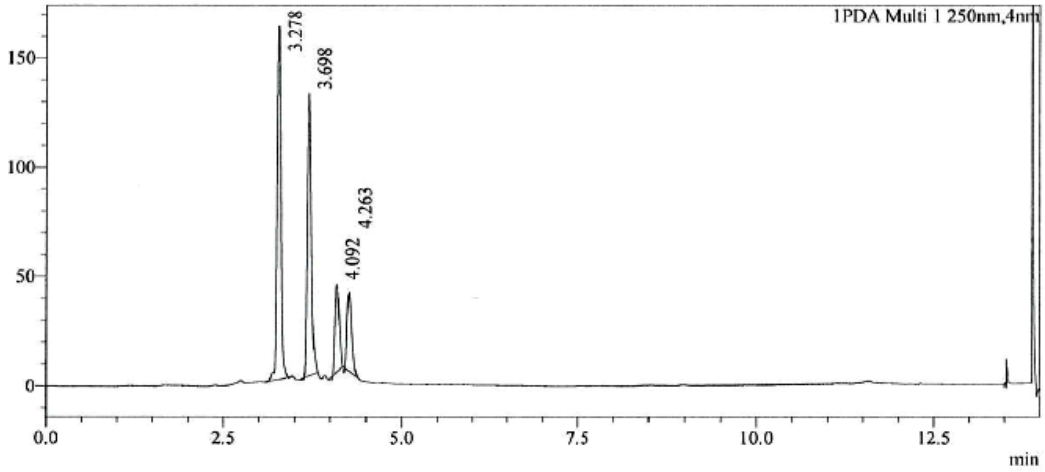


Peak Table

PDA Ch1 250nm

| Peak# | Ret. Time | Area | Height | Area% | Height% |
|---|---|---|---|---|---|
| 1 | 3.278 | 546618 | 160509 | 39.662 | 44.105 |
| 2 | 3.698 | 515486 | 127815 | 37.403 | 35.121 |
| 3 | 4.092 | 161957 | 39902 | 11.751 | 10.964 |
| 4 | 4.263 | 154129 | 35702 | 11.183 | 9.810 |
| Total | | 1378191 | 363927 | 100.000 | 100.000 |

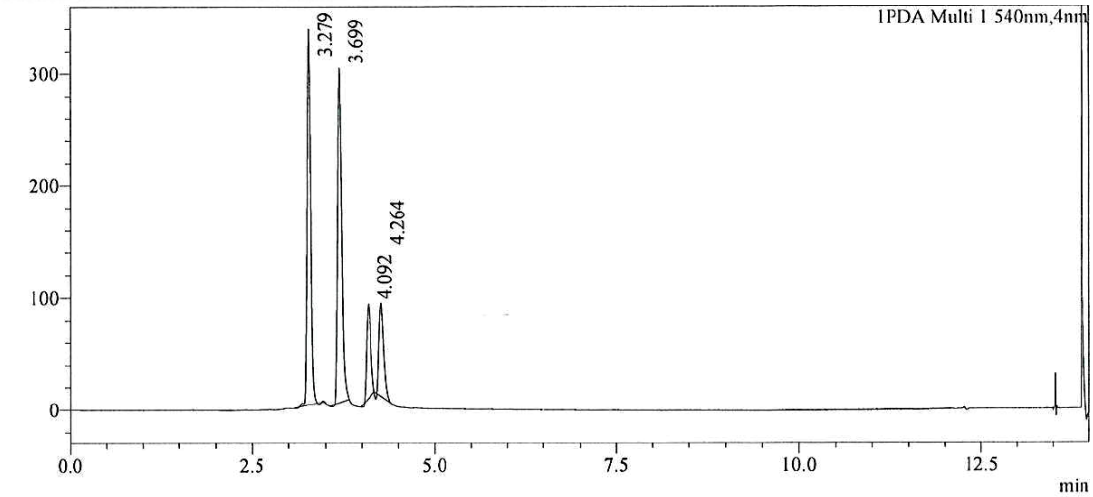


Peak Table

PDA Ch1 540nm

| Peak# | Ret. Time | Area | Height | Area% | Height% |
|---|---|---|---|---|---|
| 1 | 3.279 | 1089045 | 331812 | 36.610 | 41.748 |
| 2 | 3.699 | 1187088 | 296581 | 39.906 | 37.315 |
| 3 | 4.092 | 340825 | 84087 | 11.457 | 10.580 |
| 4 | 4.264 | 357755 | 82314 | 12.027 | 10.357 |
| Total | | 2974713 | 794795 | 100.000 | 100.000 |

Figure S18: Chromatogram of crude **3**, recorded with an UV/VIS detector set to 250nm (top) and 540nm (bottom), bandwidth 4nm each. The corresponding peak integrals are listed in the peak tables.

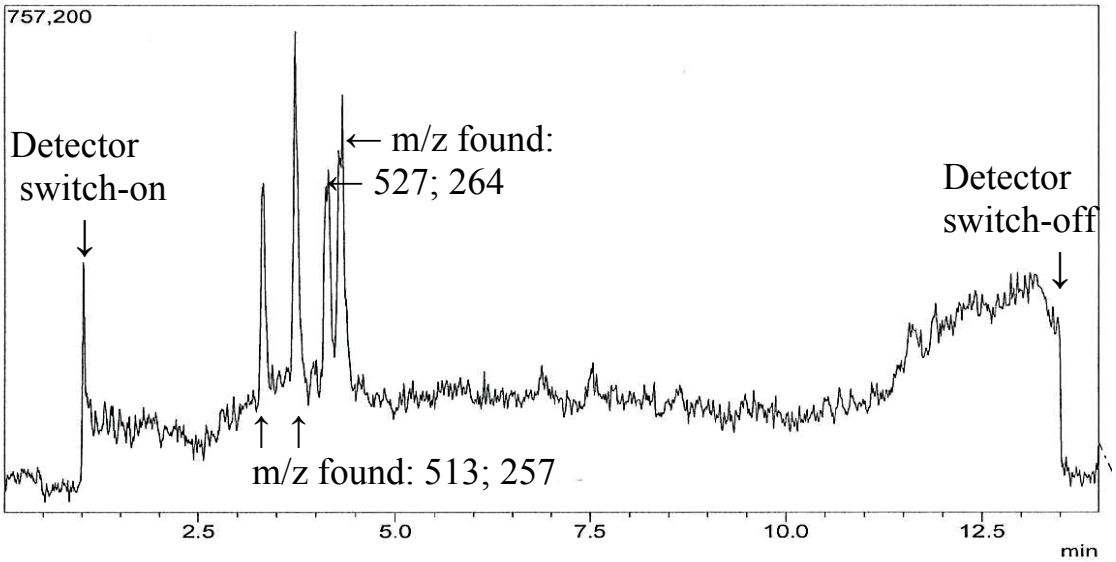


Figure S19: Total ion current chromatogram of crude **3**, recorded with an ESI-quadruple MS detector.

Gradients used for HPLC purification:

Table S1: HPLC gradient used for the purification of **1**.

| Time/min | Ratio MeOH/% | Ratio 0.1% aqueous HOAc/% | Flow rate/ml·min$^{-1}$ |
|---|---|---|---|
| 0 | 0 | 100 | 4 |
| 10 | 30 | 70 | 4 |
| 11 | 100 | 0 | 4 |
| 16 | 100 | 0 | 4 |
| 17 | 0 | 100 | 4 |
| 22 | 0 | 100 | 4 |

Table S2: HPLC gradient used for the purification of **2**.

| Time/min | Ratio MeOH/% | Ratio 0.1% aqueous HOAc/% | Flow rate/ml·min$^{-1}$ |
|---|---|---|---|
| 0 | 10 | 90 | 16 |
| 30 | 25 | 75 | 16 |
| 32 | 100 | 0 | 16 |
| 40 | 100 | 0 | 16 |

Table S3: HPLC gradient used for the purification of **3**.

| Time/min | Ratio MeOH/% | Ratio 0.1% aqueous HOAc/% | Flow rate/ml·min$^{-1}$ |
|---|---|---|---|
| 0 | 0 | 100 | 4 |
| 12 | 30 | 70 | 4 |
| 12.5 | 100 | 0 | 4 |
| 16.5 | 100 | 0 | 4 |
| 17 | 0 | 100 | 4 |
| 21 | 0 | 100 | 4 |

Gradient used for LC-MS characterisation

Table S4: Gradient used for LC-MS characterisation of **1**-**3**.

| Time/min | Ratio MeOH/% | Ratio 0.01% aqueous HCOOH/% | Flow rate/ml·min$^{-1}$ |
|---|---|---|---|
| 0 | 2 | 98 | 0.7 |
| 5 | 2 | 98 | 0.7 |
| 10 | 100 | 0 | 0.7 |
| 12 | 100 | 0 | 0.7 |
| 13 | 2 | 98 | 0.7 |